ACADEMIC PRESS

Available online at www.sciencedirect.com
SCIENCE DIRECT®

Journal of Catalysis 217 (2003) 160–171

JOURNAL OF CATALYSIS

www.elsevier.com/locate/jcat

Reactive oxo-titanium species in titanosilicate molecular sieves: EPR investigations and structure–activity correlations

D. Srinivas,* P. Manikandan, S.C. Laha, R. Kumar, and P. Ratnasamy *

National Chemical Laboratory, Pune 411 008, India

Received 14 October 2002; revised 3 February 2003; accepted 7 February 2003

Abstract

The structure of the reactive oxo-titanium species (hydroperoxo-, peroxo-, and superoxo-titanium) in titanosilicate molecular sieves (TS-1, Ti-β, amorphous Ti–SiO_2, and TiMCM-41), generated on interaction with aqueous H_2O_2 or urea–H_2O_2 adducts, was investigated by electron paramagnetic resonance (EPR) and diffuse reflectance UV–visible (DRUV–visible) spectroscopies and magnetic susceptibility measurements. Two types of superoxo-titanium species (A and B) were identified in TS-1 and amorphous Ti–SiO_2. An additional oxo species, A′, was also detected over Ti-β. TiMCM-41 generated, mainly, the B-type species. DRUV–visible spectroscopy and magnetic susceptibility measurements suggest the coexistence of both the superoxo- and hydroperoxo-titanium species. The A-type oxo-titanium species originate from the framework Ti sites having a tetrapodal $(SiO)_4Ti$ structure located inside the pores, while the B-type species originate predominantly from tripodal $(SiO)_3Ti(OH)$ structures, also located in the framework, probably at the external surface. The local structural environment of the Ti^{4+} ions, solvent, and temperature influence the concentration of these oxo-titanium species. The concentration of the A-type species decreased in the order: TS-1 > Ti-β >amorphous Ti–SiO_2. The B type varied as follows: TiMCM-41 > amorphous Ti–SiO_2 > Ti-β > TS-1. In the oxidation of styrene, the A-type species correlate with styrene oxide formation, while the presence of B-type species lead to nonselective products. Experimental evidence is given for the involvement of the hydroperoxo-titanium species in olefinic epoxidations (styrene to styrene oxide) and the superoxo-titanium in aromatic hydroxylations (phenol to hydroquinone and catechol).

Keywords: Titanosilicate molecular sieves; Reactive oxygen species; EPR; Diffuse reflectance UV–visible; Hydroperoxo-, peroxo-, superoxo-titanium; Catalytic oxidations over titanosilicates; Epoxidation of styrene

1. Introduction

Although, in the past two decades, considerable progress has been made in identifying the structure of Ti sites in titanosilicate (especially TS-1) molecular sieves, the nature of the transient, reactive oxo-species (oxo-titanium) generated during oxidation with H_2O_2 is, so far, not fully understood [1–4]. Factors controlling the chemo- and regioselectivity in specific reactions (olefinic vs allylic oxidations, for example) over TS-1, are, especially, far from well understood. An understanding of these factors will, hopefully, lead to the design and development of efficient large-pore titanosilicate molecular sieves more active than the medium-pore TS-1 in the selective oxidation of large molecules of interest to the fine chemicals industry.

The local structure of Ti is different in different titanosilicates [5–7]. EXAFS studies revealed, at least, two types of framework, tetrapodal $(SiO)_4Ti$ structures in activated TS-1 catalysts [8]. Ti in TiMCM-41 (prepared by the grafting method) possesses a tripodal $(SiO)_3Ti(OH)$ structure [9,10]. These Ti sites in different structural environments will generate reactive oxygen species having different structures and reactivities. Three types of oxo-titanium species viz., hydroperoxo-, peroxo-, and superoxo-titanium, have been invoked in oxidation reactions over titanosilicate molecular sieves with H_2O_2 [1–3]. The oxo-titanium species generated by contacting TS-1 with H_2O_2 show a characteristic absorption band in DRUV–visible spectrum in the region 300–500 nm. Geobaldo et al. [11] and Zecchina et al. [12] attributed this band to a ligand-to-metal charge transfer transition (LMCT) of a peroxo moiety interacting with a framework Ti center. In addition, vibrational spectroscopy (FT-IR and Raman) shows characteristic O–O stretching bands at 886 and 837 cm^{-1}. Tozzola et al. [13]

* Corresponding authors.
E-mail addresses: srinivas@cata.ncl.res.in (D. Srinivas), prs@ems.ncl.res.in (P. Ratnasamy).

0021-9517/03/$ – see front matter
doi:10.1016/S0021-9517(03)00060-5

assigned these bands to end-on Ti–OOH and anionic triangular Ti-peroxo moieties, respectively. Recently, Lin and Frei [14], using FT-IR spectroscopy, claimed the formation of η^2-TiOOH species absorbing at 837 and 3400 cm^{-1}. Sankar and co-workers [9,10] reported EXAFS measurements of the TiMCM-41–*tert*-butyl hydroperoxide system. These studies combined with DFT calculations [9] indicated the formation of a bidentate side-on (η^2- or η^1-) peroxo-Ti structure. Ti complexes like $(NH_4{}^+)_3[(F_5TiO_2)^{3-}]$ (where Ti is not in tetrahedral coordination) show a DRUV–visible spectrum similar to that of oxo-Ti species [11]. Hence, the structures of the type $(H^+)_2[(SiO)_4TiO_2]^{2-}$ cannot be ruled out especially in water where the H^+ can form the stable $(H_3O)^+$ species. As a matter of fact, the TS-1–H_2O_2 system is behaving as a stronger acid than H_2O_2. Earlier, Geobaldo et al. [11], based on EPR spectroscopy, had identified superoxo-Ti radical species in TS-1 samples contacted with H_2O_2 (about 2% of the Ti sites) and suggested that they formed by a side reaction of Ti–OOH and $HO^{\bullet}$ radicals. Later, Tuel et al. [15,16] and Zhao et al. [17] have also confirmed the formation of superoxo-Ti species in TS-1 catalysts. We had, earlier, identified two types of superoxo-Ti species (A and B) in TS-1 in contact with H_2O_2 [18]. Only the B-type species was detected in TiMCM-41 [18]. The effect of solvents on the nature of the oxo-titanium species and their thermal stability were also studied [18]. Bonoldi et al. [19] have, recently, reported the role of water in the formation of A and B species and theoretical calculations on the structure of these superoxo species. Their results are in agreement with our earlier report [18]. Recently, Laha and Kumar [20] have reported, in brief, on the EPR of TS-1 when reacted with urea–H_2O_2 adducts, and its catalytic properties.

We now report a comprehensive EPR investigation of oxo-titanium species generated by the interactions of aqueous H_2O_2 and urea–H_2O_2 adducts with different titanosilicates viz., TS-1, Ti-β, amorphous TiO_2–SiO_2 (denoted as Ti–SiO_2), and TiMCM-41 molecular sieves. Additionally, DRUV–visible and, for the first time, magnetic susceptibility of oxo-titanium species are also reported. Earlier, Geobaldo et al. [11], using $CuSO_4 \cdot 5H_2O$ as reference standard, found that 2% of total Ti forms superoxo-Ti species. Later, Bonoldi et al. [19] estimated the spin concentration of superoxo-Ti as 0.14% of the total Ti, using a strong pitch sample, as a reference standard. It may be noted that the linewidth and the nature of the spectra of these reference standards are different from those of superoxo-Ti species. Moreover, the concentration of the strong pitch samples usually decreases with the storage time. Hence, $CuSO_4 \cdot 5H_2O$ and pitch may not be appropriate reference standards for *quantitative* estimation of the oxo-titanium species. In the absence of a suitable standard the estimates of oxo-titanium species based on these materials as reference standards may be misleading. We have used a different, more fundamental approach for quantification using TS-1 samples with known amounts of isolated, framework Ti ions as standards. Independent estimates of the concentration of the oxo-titanium species were also made by magnetic susceptibility and DRUV–visible spectroscopy. This combined study reveals that *significant* amounts of both the superoxo-, and hydroperoxo-/peroxo-titanium species are present under our experimental conditions. The relative concentrations of the various oxo-titanium species depend on silicate structure, temperature, and solvent. Evidence is provided for the involvement of the hydroperoxo-titanium species in olefinic epoxidations (styrene to styrene oxide) and the superoxo-titanium in aromatic hydroxylations (phenol to hydroquinone and catechol).

2. Experimental

2.1. Synthesis

TS-1 was prepared according to the reported procedure of Laha and Kumar [20] and Kumar et al. [21,22]. A typical gel composition of TS-1 was 1 TEOS:0.5 TPAOH: 0.033 TBOT:0.067 H_3PO_4:25 H_2O. Tetraethyl orthosilicate (TEOS) was used as the source of silica and tetrabutyl orthotitanate (TBOT) as the source of titanium. H_3PO_4 was used as a promoter. Tetrapropylammonium hydroxide (TPAOH, 20 wt% aqueous solution) was used in the preparation of TS-1 to maintain the pH of the gel.

Al-free Ti-β was synthesized according to the procedure of Blasco et al. [23]. In a typical synthesis, 80 g of tetraethyl orthosilicate, 91.26 g of tetraethylammonium hydroxide (TEAOH, 34.8% in H_2O), 15.45 g of H_2O_2 solution (30% in water), and 1.42 g deionized water were mixed in a polypropylene beaker, with stirring. To this, 3.50 g of tetraethyl orthotitanate was added, dropwise, under stirring. The titanium source was added directly from the bottle to avoid prehydrolysis and, thus, TiO_2 formation. The titanium source dissolved to yield a yellow, clear solution. Stirring was continued by heating the solution at 323–333 K and by gently purging with nitrogen to remove alcohols from the gel mixture. The resulting solution was loaded into a Parr autoclave and 10.78 g of hydrofluoric acid (40% in water) was added to the solution dropwise, to obtain a yellow solid gel. The synthesis gel composition of Ti-β was 1 SiO_2: 0.02 TiO_2:0.56 TEAOH:0.34 H_2O_2:7.6 H_2O:0.56 HF. The gel was heated to 413 K, for 14 days, under rotation (60 rpm). The resulting solid was filtered, washed with deionized water, dried, and calcined in static air, at 823 K, for 8 h, to remove the template.

In the preparation of TiMCM-41, TBOT and fumed silica were used as Ti and Si sources, respectively. As H_3PO_4 was used as promoter in the synthesis of TiMCM-41 sample, excess TMAOH was used to maintain the pH of the gel mixture. TiMCM-41 was prepared as reported earlier [24] using the molar gel composition of 1 SiO_2:0.02 TiO_2:0.4 TMAOH:0.21 CTABr:125 H_2O:0.1 H_3PO_4.

The amorphous titanosilicate (denoted as amorphous Ti–SiO_2) was prepared according to the procedure of Keshavaraja et al. [25].

2.2. Characterization procedures

The phase purity and framework substitution of Ti in TS-1, Ti-β, and TiMCM-41 were established, as reported earlier [20,24], using X-ray diffraction (Rigaku D MAX III VC), energy dispersive X-ray analysis (Kevax equipment attached to a JEOL JSM-5200), scanning electron microscopy (Leica Stereoscan 440), transmission electron microscopy (JEOL JEM-1200EX), and diffuse reflectance UV–visible (Shimadzu UV-2101 PC and UV-2550) and FT-IR (Shimadzu FTIR-8201 PC) spectroscopies. Si/Ti ratios in TS-1, Ti-β, TiMCM-41 and amorphous Ti–SiO_2 were found to be 32, 50, 52, and 54, respectively.

EPR spectra were recorded on a Bruker EMX X-band spectrometer operating at 100 kHz field modulation. The microwave frequency was calibrated using a frequency counter of the microwave bridge ER 041 XG-D. The variable temperature measurements (80–348 K) were carried out using a Bruker BVT 3000 temperature controller accessory. The Bruker Simfonia software package was used in the spectral simulations and WINEPR to calculate the spectral intensity by the double integration method. The EPR spectra were recorded taking the samples in suprasil quartz tubes. Prior to the EPR measurements, the samples were activated at 373 K, under air. Magnetic susceptibility measurements were done on a Lewis coil force magnetometer (Series 300 George Associates, USA). Magnetic susceptibilities of TS-1 and TS-1 + H_2O_2 samples were estimated at 298 K.

2.3. Sample preparation for EPR

In the experiments with H_2O_2, a known amount of the solvent (0.4 ml) was added to a known amount of titanosilicate (45 mg), such that the catalyst was completely soaked in the solvent. Then 0.1 ml of aqueous H_2O_2 (30%) was added. The catalyst changed its color from white to yellow.

In the experiments with urea–H_2O_2 adduct, 50 mg of titanosilicate was gently mixed with 100 mg of urea–H_2O_2 adduct. In this case also the color of sample changed from white to yellow. In the study of solvent effect, these samples were then exposed to the vapors of H_2O, CH_3OH, $(CH_3)_2CO$, and CH_3CN, for a specified period of 5–15 min.

2.4. Epoxidation of styrene

The epoxidation of styrene was carried out in a batch reactor, over titanosilicates, in different solvents, using aqueous H_2O_2 or urea–H_2O_2 as the oxidant. In a typical reaction, 2.08 g of styrene, 2.08 g of solvent, 0.416 g of the catalyst, and 5 mmol of aqueous H_2O_2 or urea–H_2O_2 were taken. The reaction mixture was heated to 313 K, under stirring. After completion of the reaction, the organic layer was collected by centrifugation and analyzed using a HP 6890 gas chromatograph (HP 101 methyl silicone fluid, 50 m × 0.2 mm × 0.2 μm thickness). The products were identified by GC-IR (Perkin-Elmer, GC-IR 2000) and GC-MS (Shimadzu, GCMS-QP 2000A).

3. Results and discussion

3.1. Interaction of titanosilicates with aqueous H_2O_2

3.1.1. Effect of silicate structure

On addition of aqueous H_2O_2, the calcined titanosilicate molecular sieves showed a rhombic-type EPR spectrum corresponding to superoxo-titanium species ($Ti(O_2^{-\cdot})$) [11, 15–20,26,27]. The signals (Fig. 1) of TS-1 and Ti-β were narrow, while those of amorphous Ti–SiO_2 and TiMCM-41, as expected, were broad. Spectral simulations revealed that TS-1 contains two types of $Ti(O_2^{-\cdot})$ species, A and B, with species A being more abundant. Ti-β contains an additional species, A′. Their concentration (in Ti-β) decreases in the order, B > A > A′. Amorphous Ti–SiO_2 also contains both the A- and B-type species; the signals were broad and barely resolved. TiMCM-41 contains mainly the B-type species. Thus, the silicate structure has a definite influence on the type of Ti-oxo species formed and their concentration. These species differ, mainly, in their g_z value (2.0320 for A′, 2.0275(7) for A, and 2.0243(8) for B, respectively); g_x and g_y are almost the same for all samples (Table 1). The linewidth of the g_z signal is different for different $Ti(O_2^{-\cdot})$ species. Species B has a larger linewidth (∼ 3.8 G) than the others (1.0 G for A′ and 1.8 G for A). The intensity of these signals increased with Ti content, confirming their origin from Ti-containing species. It is noted here that these

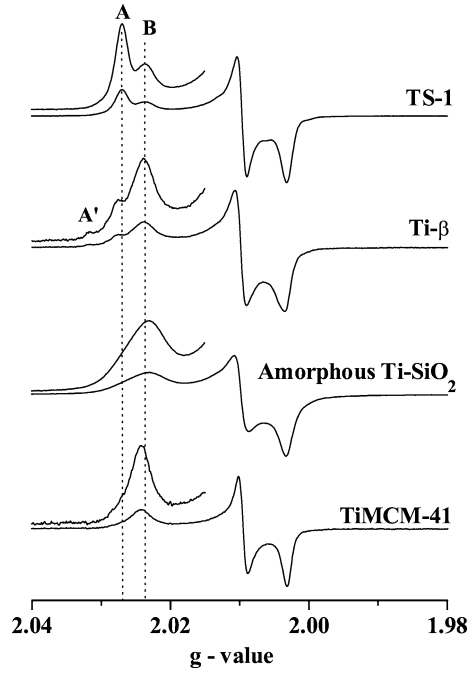

Fig. 1. EPR spectra (at 210 K) of titanosilicates interacted with aqueous H_2O_2; g_z region at higher gain (×5) is shown; the peaks corresponding to A′, A, and B are indicated.

Table 1
EPR g values of Ti($O_2^{-\cdot}$) species in different titanosilicates generated by interaction with aqueous H_2O_2 or urea–H_2O_2 adducts

System	Species	g_z	g_y	g_x	Δ (cm^{-1})
TS-1 + H_2O_2	A	2.0266	2.0090	2.0023	11110
	B	2.0238	2.0090	2.0023	12558
TS-1 + urea–H_2O_2	A′	2.0300	2.0101	2.0035	9747
	A	2.0275	2.0101	2.0035	10714
	B	2.0242	2.0101	2.0035	12329
	C	2.0206	2.0101	2.0035	14754
Ti-β + H_2O_2	A′	2.0310	2.0100	2.0035	9407
	A	2.0278	2.0100	2.0035	10588
	B	2.0257	2.0100	2.0035	11538
Ti-β + urea–H_2O_2	A′	2.0324	2.0092	2.0027	8970
	A	2.0271	2.0092	2.0027	10887
	B	2.0235	2.0092	2.0043	12736
Amorphous Ti–SiO_2	A	2.0274	2.0100	2.0031	10756
+ H_2O_2	B	2.0239	2.0100	2.0031	12500
Amorphous Ti–SiO_2	A	2.0267	2.0099	2.0033	11066
+ urea–H_2O_2	B	2.0235	2.0099	2.0047	12736
	C	2.0218	2.0099	2.0033	13846
TiMCM-41 + H_2O_2	B	2.0240	2.0093	2.0027	12442
TiMCM-41	A	2.0280	2.0096	2.0032	10506
+ urea–H_2O_2	B′	2.0252	2.0096	2.0032	11790
	B	2.0232	2.0096	2.0046	12919

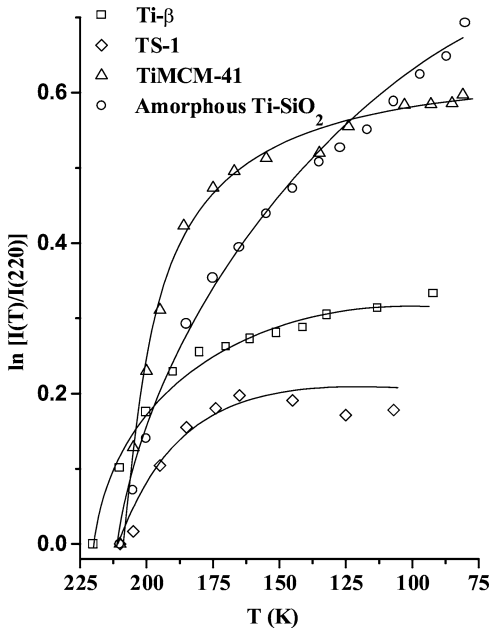

Fig. 2. Variation of total EPR intensity per mole of Ti as a function of temperature (ln[$I(T)/I(220)$] vs T) in different titanosilicates in contact with aqueous H_2O_2.

paramagnetic oxo-titanium species were not observed in the interactions of H_2O_2 with either silicalite-1 or anatase in agreement with the results of Zhao et al. [17].

3.1.2. Effect of temperature

Fig. 2 shows the variation of the relative spectral intensity per mole of Ti, (ln($I(T)/I(220)$)), of different titanosilicates as a function of temperature. Here, $I(220)$ is the total

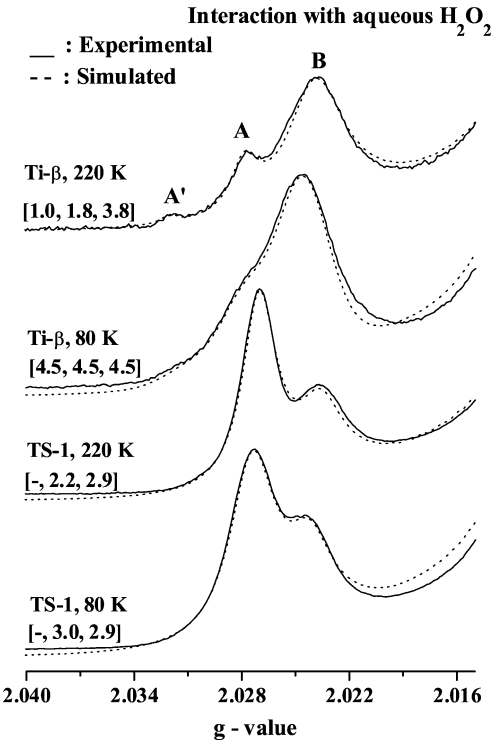

Fig. 3. EPR spectra (in g_z region) of TS-1 and Ti-β in contact with aqueous H_2O_2 showing the effect of temperature on the linewidth and intensity. The linewidth parameters of A′, A, and B are given in parentheses. TS-1 does not contain A′.

EPR signal intensity at 220 K and $I(T)$ is that at temperature T. This value increased steeply with a decrease in the temperature. Below $\sim$ 175 K, the increase was less marked. Amophous Ti–SiO_2 showed a different behavior, the signal intensity increased continuously with lowering of the temperature. The total spectral intensity of different titanosilicates (at 80 K) decreased in the order: amorphous Ti–SiO_2 > TiMCM-41 > Ti-β > TS-1.

The experimental and simulated curves of TS-1 and Ti-β, in the g_z region, at 80 and 220 K (Fig. 3) agree reasonably well. The linewidth of the individual signals A′, A, and B (Fig. 3) increased at lower temperatures. This broadening was more significant in Ti-β than in TS-1. The broadening was maximum for A′ (from 1.0 to 4.5 G in Ti-β), intermediate for A (from 1.8 to 4.5 G in Ti-β and 2.2 to 3.0 G in TS-1), and minimum for B-type Ti($O_2^{-\cdot}$) species (from 3.8 to 4.5 G in Ti-β and no change in TS-1). A marginal shift in the signals to a higher g value and a reduction in the intensity of A′ and A were also noted at lower temperatures.

3.1.3. Effect of solvent

Fig. 4 demonstrates the effect of solvents (H_2O, CH_3OH, CH_3CN, and $(CH_3)_2CO$) on the EPR spectra of TS-1 and Ti-β. In the case of TS-1, species A was more predominant than B when H_2O was the solvent. In all the other solvents B was more intense. The intensity ratio, A/B, in different solvents decreased in the order: CH_3CN > CH_3OH >

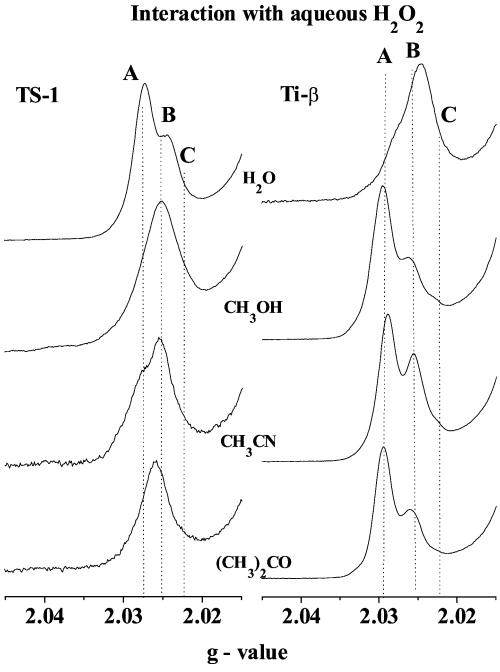

Fig. 4. Effect of solvents on the concentration of A and B in TS-1 and Ti-β in contact with aqueous H_2O_2. The curves correspond to the g_z region of EPR spectra at 80 K.

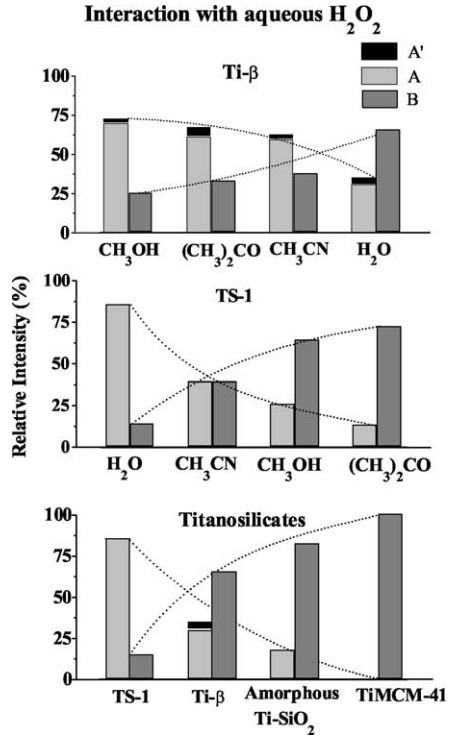

Fig. 5. Relative EPR intensity (at 80 K) of Ti($O_2^{-}\cdot$) species (A′, A, and B) generated by contact with aqueous H_2O_2, (bottom) in different titanosilicates, (middle) TS-1 in different solvents, (top) Ti-β in different solvents.

$(CH_3)_2CO$. In the case of Ti-β, species B was more predominant than A in H_2O. In other solvents, A was more intense. The ratio A/B, in Ti-β, decreased in the order: $CH_3OH > (CH_3)_2CO > CH_3CN$. An additional species, C, was also detected in the case of Ti-β (Fig. 4) whose concentration was smaller than that of A and B. The total spectral intensity was lower in TS-1 than in Ti-β (Fig. 4). The EPR parameters in different solvents are listed in Table 2.

3.1.4. Concentration of Ti($O_2^{-}\cdot$) species

Fig. 5 shows the concentration profile of the different Ti($O_2^{-}\cdot$) species (A′, A, and B) in different titanosilicates and solvents. The amount of A decreased in the titanosilicates in the order: TS-1 $\gg$ Ti-β > amorphous Ti–SiO_2. Species A was absent in TiMCM-41. Species B, on the other hand, decreased in the order: TiMCM-41 > amorphous Ti–SiO_2 > Ti-β > TS-1. A′ was present only in Ti-β. In different solvents, the concentration of A in TS-1 decreased in the order: $H_2O > CH_3CN > CH_3OH > (CH_3)_2CO$. The concentration of B, however, varied in the reverse order (Fig. 5). In the case of Ti-β, the concentration of A + A′ varied in the order: $CH_3OH \approx (CH_3)_2CO > CH_3CN > H_2O$. Thus, the structure of the titanosilicate and the dimension and coordinating ability of the solvent molecules influence the type of oxo-Ti species formed.

Table 2
EPR parameters of Ti($O_2^{-}\cdot$) in different solvents

Solvent	Species	TS-1			Ti-β			TiMCM-41		
		g_z	g_y	g_x	g_z	g_y	g_x	g_z	g_y	g_x
CH_3CN	A′	–	–	–	2.0340	2.0101	2.0032	–	–	–
	A	2.0264	2.0090	2.0023	2.0286	2.0101	2.0032	2.0265	2.0093	2.0027
	B	2.0235	2.0090	2.0023	2.0252	2.0101	2.0032	2.0240	2.0093	2.0027
	C	2.0220	2.0090	2.0023	–	–	–	–	–	–
$(CH_3)_2CO$	A′	–	–	–	2.0345	2.0107	2.0038	–	–	–
	A	2.0265	2.0087	2.0018	2.0287	2.0107	2.0037	–	–	–
	B	2.0235	2.0087	2.0018	2.0287	2.0107	2.0037	2.0245	2.0093	2.0026
	C	2.0210	2.0087	2.0018	–	–	–	–	–	–
CH_3OH	A′	–	–	–	2.0320	2.0101	2.0034	–	–	–
	A	2.0260	2.0090	2.0023	2.0289	2.0101	2.0034	–	–	–
	B	2.0235	2.0090	2.0023	2.0257	2.0101	2.0034	2.0233	2.0090	2.0026
	C	2.0220	2.0090	2.0023	–	–	–	–	–	–

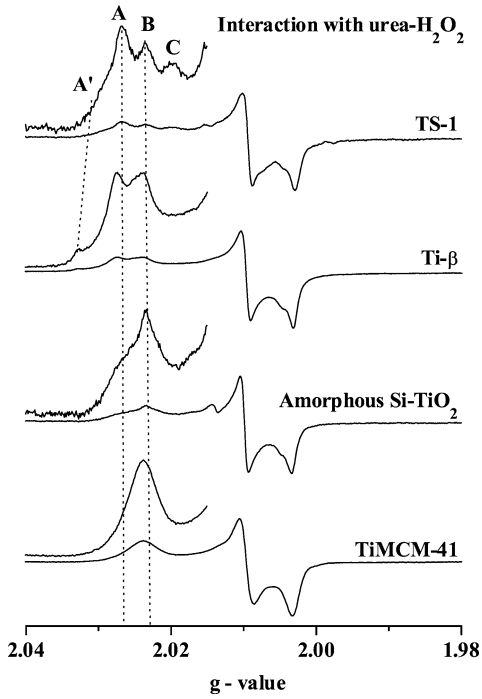

Fig. 6. EPR spectra (at 298 K) of different titanosilicates interacted with urea–H_2O_2; g_z region at higher gain (×5) is shown. The signals due to A′, A, and B are marked by dotted lines.

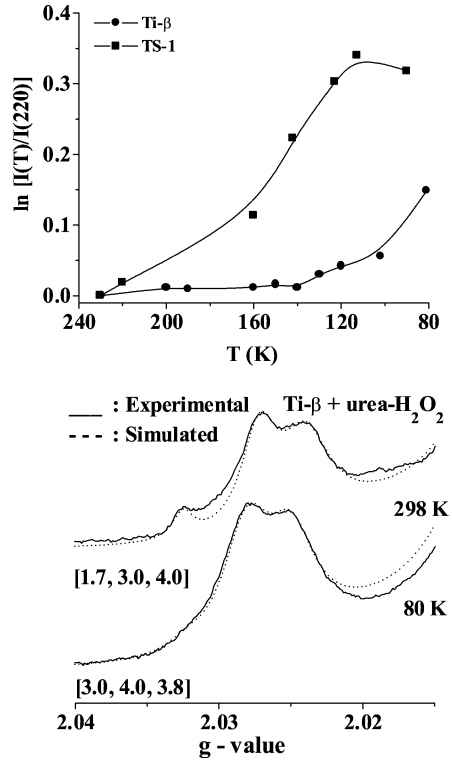

Fig. 7. Variation of EPR intensity per mole of Ti as a function of temperature ($\ln[I(T)/I(220)]$ vs T) in TS-1 and Ti-β interacted with urea–H_2O_2 (top). EPR spectra (in g_z region) of Ti-β + urea–H_2O_2 showing the effect of temperature (298 and 80 K) on the linewidth and intensity. The linewidth parameters of A′, A, and B are given in parentheses.

3.2. Interaction of titanosilicates with urea–H_2O_2 adducts

3.2.1. Effect of silicate structure

Fig. 6 shows the EPR spectra of the titanosilicate molecular sieves mixed with urea–H_2O_2 adducts. The spectra are rather different than those observed with aqueous H_2O_2 (compare Figs. 6 and 1). Only in the case of Ti-MCM-41 some resemblances are evident (Table 1). TS-1 contains all the four superoxo-Ti species, with their concentrations varying in the order: A > B > A′ > C. Ti-β contains only A′, A, and B, with A′ being less intense than A or B over Ti-β. A′ species is more abundant when Ti-β is contacted with urea–H_2O_2. Amorphous Ti–SiO_2 contains mostly A and B along with small amounts of C. TiMCM-41 contains mainly B.

3.2.2. Effect of temperature

The variation of $\ln(I(T)/I(220))$ as a function of T is plotted in Fig. 7 (top). TS-1 and Ti-β with urea–H_2O_2 behave differently than with aqueous H_2O_2 (compare Fig. 7 (top panel) and Fig. 2). The relative spectral intensity of TS-1 increased at lower temperatures down to ∼ 120 K and then remained almost constant. With aqueous H_2O_2 this change occurred at higher temperatures (∼ 175 K; see Fig. 2). The spectral intensity of Ti-β was almost invariant up to ∼ 160 K and then increased at lower temperatures (Fig. 7, top). The experimental and the simulated curves of Ti-β with urea–H_2O_2, in the g_z region, at 80 and 220 K are shown in Fig. 7 (bottom). At lower temperatures, as observed in the case of aqueous H_2O_2, the linewidth of the individual species increased (from 1.7 to 3.0 G for species A′ and from 3.0 to 4.0 G for A), the signals shifted marginally to higher g values and the intensity of A and A′ decreased.

3.2.3. Effect of solvents

TS-1 and Ti-β were initially reacted with urea–H_2O_2 and then exposed to the vapors of CH_3OH, CH_3CN, and $(CH_3)_2CO$. A and B were the predominant species. The urea–H_2O_2-treated TS-1 showed broader, partially resolved signals as compared to the H_2O_2-treated samples (compare Figs. 4 and 8), indicating a greater heterogeneity of magnetically inequivalent Ti($O_2^{-\cdot}$) ions in the presence of urea–H_2O_2. Ti-β exhibited narrow signals as compared to TS-1 (Fig. 8). The intensity ratio A/B of urea–H_2O_2-treated Ti-β varied in the order: H_2O > CH_3OH > CH_3CN > $(CH_3)_2CO$. A′ was also significant in H_2O-exposed Ti-β. The concentration of C was low in all the solvents. The relative concentrations of A′, A, and B in TS-1 and Ti-β are shown in Fig. 9. The amount of A′ + A decreased in the order: TS-1 > Ti-β > amorphous Ti–SiO_2 ≫ TiMCM-41 (Fig. 9, bottom). In TS-1, in different solvents, it decreased in the order: $(CH_3)_2CO$ > CH_3CN ∼ CH_3OH (Fig. 9, middle). Species B showed a reverse trend. The variation in the concentration of [A′ + A] and [B] in Ti-β, in different solvents, was negligible (Fig. 9, top).

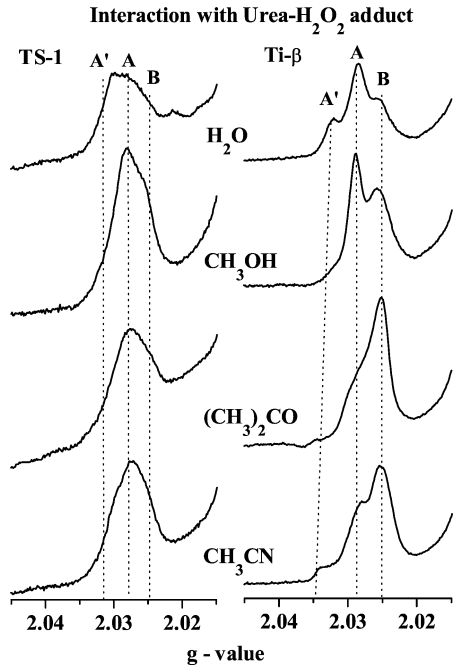

Fig. 8. PER spectra (at 80 K) of solvent exposed TS-1/Ti-β + urea–H_2O_2 systems.

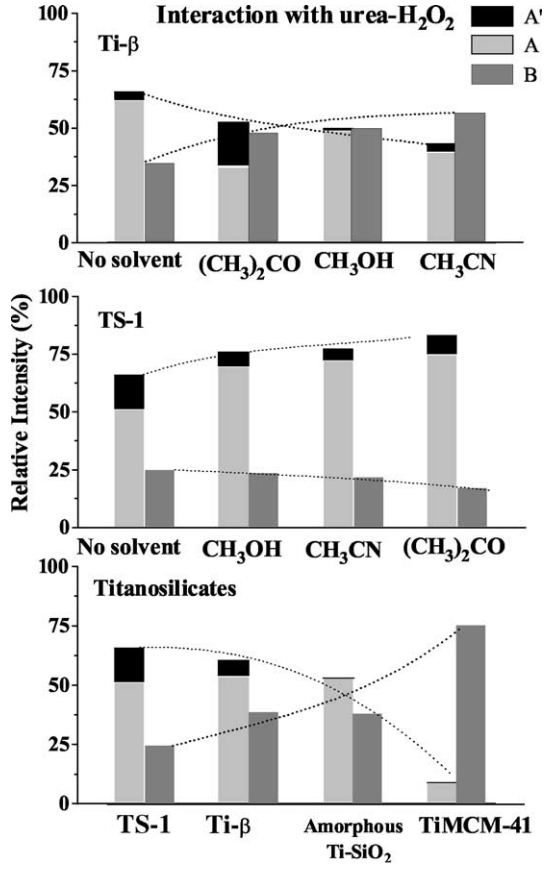

Fig. 9. Relative EPR intensity of Ti($O_2^{-\cdot}$) species (A′, A, and B) in titanosilicates interacted with urea–H_2O_2: (bottom) in different titanosilicates (at 298 K), (middle) TS-1 in different solvents (at 80 K), (top) Ti-β in different solvents (at 80 K).

3.3. Structure of Ti($O_2^{-\cdot}$) species

The XRD, DRUV–visible, and FT-IR spectroscopic studies confirm that most of the Ti in TS-1, Ti-β, and TiMCM-41 are in framework tetrahedral positions [18]. No extraframework anatase was detected. During the reaction with alkyl hydroperoxides, EXAFS studies had indicated that Ti expands its coordination number from 4 to 5 or 6 depending on their location and the nature of the titanosilicate [8–10]. Coordination of $O_2^{-\cdot}$ with a metal ion (like Ti) removes the degeneracy of the highest occupied molecular orbital π_g into $\pi_g{}^x$ and $\pi_g{}^y$ orbitals that are separated by Δ [28]. The g_z value of the Ti($O_2^{-\cdot}$) superoxo anion is sensitive to the Ti–O bond length, and the oxidation state, coordination number, and local geometry of Ti [28]. The stronger the Ti–($O_2^{-\cdot}$) bond, the lower the g_z value and the higher the Δ values of the superoxo anion. Using the g values (Table 1), the energy gap (Δ value) was estimated as described earlier [18]. Δ decreased for different superoxo-Ti species in the order: C > B > A > A′ (Table 1). Thus, the strength of the Ti–($O_2^{-\cdot}$) bond decreases in the order: C > B > A > A′. The O–O bond strength, on the other hand, will follow the reverse order since a stronger binding of the O atoms to the Ti ion weakens the intramolecular O–O bonding. The g_z parameter of the A-type species decreased in the order: TS-1 > Ti-β > amorphous Ti–SiO_2. Hence, the O–O bond strength of Ti($O_2^{-\cdot}$) in these silicates should vary in the same order. As the lability of the O–O bonds influences its reactivity, the different Ti($O_2^{-\cdot}$) species are expected to exhibit different reactivities. The observed differences in the activity and chemoselectivity of the different titanosilicates probably arise from such differences in the strength of the O–O bond in the Ti-oxo species formed over them in the presence of oxidants like H_2O_2, urea–H_2O_2 or $H_2 + O_2$. Although the calculation of Δ values is based on a purely ionic model, they are also relevant for the metal superoxide complexes. Interestingly, they also correlate well with the catalytic activity data.

The EXAFS studies [8] on TS-1 catalysts had revealed a tetrapodal coordination for Ti. Gleeson et al. [8] have divided the $(SiO)_4Ti$ units into two groups, one group with three Ti–O–Si bond angles at 140° and one Ti–O–Si at 160° and the other with two Ti–O–Si bond angles at 140° and the remaining two at 160°. In the case of TiMCM-41, prepared by a grafting method, a tripodally coordinated Ti species with coordinated hydroxyl group was also observed [9,10]. Such a structure cannot be ruled out even in other titanosilicates (like TS-1 and Ti-β) with high Ti content or surface defects. The different Ti($O_2^{-\cdot}$) species, perhaps, correspond to oxo species formed over these different Ti sites. Depending on the coordination number (5 or 6) of Ti in the Ti($O_2^{-\cdot}$) species, different types of (A′, A), (B′, B), and C species will be formed. The A and B species, revealed by our EPR studies, are probably formed by reaction of H_2O_2 with the tetra- and tripodal Ti ions indicated by EXAFS [8–10]. Zhao et al. [17] had also observed the two types

of $Ti(O_2^{-\cdot})$ species A and B in TS-1 + H_2O_2 system. The former (A) was attributed to framework Ti and the latter (B) to extraframework species. Since in our samples (Si/Ti = 30–80), the ratio of A and B was independent of the Ti content, we would like to attribute the A and B signals to the oxo species formed on tetrapodal and tripodal Ti ions, respectively, in framework positions [9,10]. Bonoldi et al. [19] have also arrived at the same conclusions.

The intensity of the EPR signal of a paramagnetic sample should vary linearly with $1/T$ [29]. The total spectral intensity of our titanosilicates exhibited a different behavior below 175 K (Fig. 2); the rise in intensity was marginal below 175 K. This can happen if a part of the EPR-active $Ti(O_2^{-\cdot})$ is converted into an EPR-inactive oxo-titanium species, such as hydroperoxides/peroxides, below 175 K. The onset of antiferromagnetic resonance may be an alternative explanation for the phenomenon observed in Fig. 2. However, in view of the very low concentration of Ti ions in the sample, antiferromagnetic coupling between two adjacent $O_2^{-\cdot}$ on two neighboring Ti sites is considered unlikely. It may be recalled that the UV–visible spectra of our TS-1 sample confirm the predominant concentration of *isolated*, tetrahedrally coordinated, Ti ions in them. The hydroperoxo-/peroxo-titanium species are more stable at low temperatures and the superoxo species are stable at higher temperatures. The stabilization of the EPR-inactive hydroperoxo/peroxo-titanium species at lower temperatures is also in agreement with the DFT calculations of Sankar et al. [9]. It may be noted from Fig. 2 that the overall spectral intensity per mole of Ti decreased among titanosilicates in the order: amorphous Ti–SiO_2 > TiMCM-41 > Ti-β > TS-1, suggesting that a larger amount of oxo-titanium species is in the form of EPR-inactive hydroperoxo/peroxo-titanium in TS-1, while the EPR-active superoxo-titanium predominates in TiMCM-41 and amorphous Ti–SiO_2. We had demonstrated earlier [18] that solvent also influences the superoxo–hydroperoxo conversion and their concentration. Weakly polar CH_3CN stabilized the hydroperoxo/peroxo-titanium species, while the more polar CH_3OH stabilized the superoxo-titanium species [18]. The overall signal intensity variation with temperature was different in urea–H_2O_2 adducts of TS-1 and TiMCM-41. In the case of TS-1–urea–H_2O_2, the conversion of the superoxo to the hydroperoxo/peroxo species takes place at still lower temperatures (120 K against 175 K observed in the case of TS-1–H_2O_2 system (Fig. 2)). In TiMCM-41–urea–H_2O_2 the spectral intensity increased with lowering of temperature even up to 80 K. Thus, urea promotes the stability of the superoxo-titanium species. The variation of intensity ratio (A/B) in different solvents (Figs. 4 and 9) is also, probably, due to this factor. In our earlier study [18], based on the variable temperature experiments at high temperature (298–348 K), we found that the stability of superoxo species varies in the order: B > A > C in agreement with Zhao et al.'s [17] and Bonoldi et al.'s [19] reports.

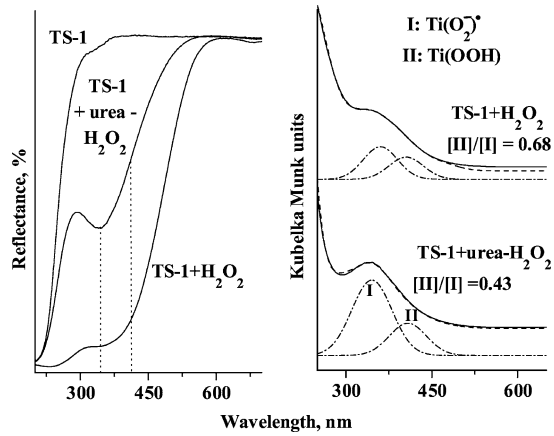

Fig. 10. Diffuse reflectance UV–visible spectra of TS-1 + aqueous H_2O_2 and TS-1 + urea–H_2O_2 at 298 K: (left) reflectance spectra, (right) absorbance spectra (in Kubelka Munk units); —, experimental; – –, simulated; · – · –, deconvoluted bands (only bands I and II are shown for clarity).

To probe further the coexistence of superoxo- and hydroperoxo/peroxo-titanium species we have carried out DRUV–visible studies on TS-1 and TiMCM-41 samples in contact with aqueous H_2O_2 and urea–H_2O_2. The influence of solvents was also investigated. Typical spectra of TS-1 in the reflectance mode and Kubelka Munk (absorption) units are shown in Fig. 10 (left and right panels, respectively). Before contact with H_2O_2 the characteristic TS-1 band appeared at 208 nm. After the interaction it shifted to 270 nm (Fig. 10, see the left panel). Such a shift was not observed in samples interacted with urea–H_2O_2, suggesting the influence of solvent (water) and formation of the pentacoordinated Ti species in the presence of H_2O [11,30]. Weak coordination of water in TS-1 was identified by others, in the EXAFS study [5–7]. In addition to this characteristic peak, a broad, asymmetric band was also observed in the region 300–500 nm in the samples contacted with H_2O_2 and urea–H_2O_2 (Fig. 10). Spectral simulations revealed that this band can be deconvoluted, into two bands I and II attributable to superoxo-titanium ($Ti(O_2^{-\cdot})$) and hydroperoxo/peroxo-titanium (Ti(OOH)) species, respectively. Bands I and II in TS-1 + aqueous H_2O_2 occur at 360 and 405 nm, respectively. In TS-1 + urea–H_2O_2 they occur at 345 and 408 nm, respectively. In both the H_2O_2 and urea–H_2O_2 systems, the band of superoxo-titanium species is more intense than that of hydroperoxo/peroxo-titanium species. Their intensity ratio is higher in the case of TS-1 + H_2O_2 than in TS-1 + urea–H_2O_2 system. The characteristic oxo-Ti bands overlap with the intense band. We deconvoluted the spectra by taking into account all the possible bands including the strong one at lower wavelength. The simulated spectrum (dashed line; Fig. 10) agrees well with the experimental spectrum (solid line, Fig. 10). The intensities and band positions estimated from the spectral deconvolution are, hence, expected to be reasonably accurate.

An attempt was made to compare the relative concentrations of the hydroperoxo-/peroxo and superoxo-titanium

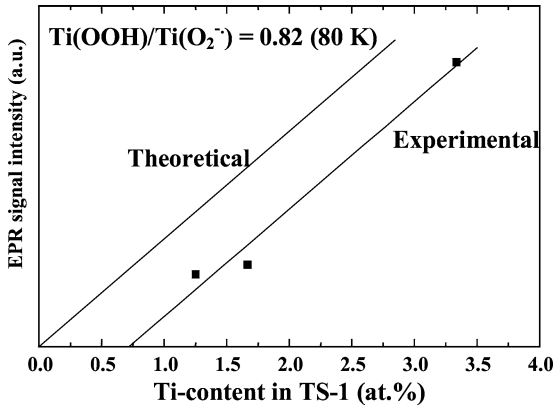

Fig. 11. Total EPR signal intensity vs Ti content in TS-1 samples.

species obtained from EPR and UV–visible spectroscopies. The "theoretical" line passing through the origin in Fig. 11 was computed on the assumption that all the Ti ions in the sample react with H_2O_2 forming *only* the paramagnetic superoxo species. For the "experimental" line in Fig. 11, the intensity of the EPR signal varies linearly with the Ti content in the various TS-1 samples. This line, however, does not pass through the origin (Fig. 11). If all the Ti in TS-1 had formed the paramagnetic Ti-superoxo species the "experimental" line would have passed through the origin and coincided with the "theoretical" line. It may be recalled that all the Ti ions in the chosen samples (Si/Ti = 30, 60, and 80) are isolated and in framework positions (XRD, FT-IR, and UV–visible analyses). Thus, they are expected to interact with H_2O_2 and form either paramagnetic superoxo or diamagnetic peroxo-Ti species. Thus, only a part of the Ti ions form paramagnetic superoxo-Ti species and the rest form diamagnetic hydroperoxo/peroxo-Ti species. From the difference in the "theoretical" and "experimental" EPR intensity values (Fig. 11) the amounts of Ti-hydroperoxo and Ti-superoxo species were estimated to be 45 and 55%, respectively, at 80 K. In the absence of a suitable reference standard we believe that this method of estimation of oxotitanium species is more reliable. From the area of the *UV–visible bands* (*II and I*), the ratio of Ti(OOH)/Ti($O_2^{-\cdot}$) in TS-1 + aqueous H_2O_2 system was found to be 0.66. This value is similar to the value (0.82) estimated independently from EPR spectroscopy. Thus, significant amounts of superoxo-species are generated on interacting titanosilicates with H_2O_2.

An additional, independent estimate of the concentration of paramagnetic superoxo and diamagnetic hydroperoxo/peroxo-titanium species was also made from magnetic susceptibility measurements using a Lewis coil force magnetometer. Magnetic susceptibilities of TS-1 and TS-1 + H_2O_2 samples were estimated at 298 K. In a typical experiment, with a magnetic field gradient of 8.77 G/cm-amp, applied magnetic field was varied from 12,000 to 0 G. Force felt by the sample at different fields was measured. Magnetic susceptibility was calculated using a least-squares fit program and the formula $F = 1.02 \times 10^{-3} \chi m H G$. Here, χ is the gram magnetic susceptibility of the sample, m is the mass of the sample in grams, G is the field gradient magnitude, H is the applied magnetic field, and F is the force in grams. The constant term 1.02×10^{-3} is the conversion factor from dynes to grams. The effective susceptibility of TS-1 + H_2O_2 sample was determined after applying the diamagnetic correction for TS-1, H_2O, and H_2O_2. The gram susceptibility of Ti in TS-1 + H_2O_2 was estimated to be 5.5×10^{-6} emu/g, which corresponds to an effective magnetic moment of 0.79 BM. If all the Ti in the sample forms superoxo species on interaction with H_2O_2 the effective magnetic moment should have been 1.73–1.78 BM. The concentration of superoxo-Ti species is, thus, about 45% of the total Ti, comparable to the values found by EPR (55%) and electronic spectroscopies. The remaining fraction is, presumably, the diamagnetic hydroperoxo-/peroxo-Ti species. H_2O_2 can be a potential source of many radicals, e.g., OH and O_2H. However, EPR spectroscopy did not reveal the presence of any of these radicals, indicating their concentration to be not very significant. They are, perhaps, highly unstable. Thus, their contribution to the total paramagnetic magnetic susceptibility is negligible.

The conversion of hydroperoxide/peroxide to superoxide is a one-electron redox reaction and requires the presence of transition metals having accessible multiple oxidation states as in biological Fe or Mn clusters (e.g., Fe(II, III, IV) clusters of monooxygenase or the Mn(II, III, IV) clusters of photosystems). Ti is usually not reduced at ambient temperatures. The various possibilities that could facilitate the transformation of hydroperoxo/peroxo to superoxo species are:

1. Homolysis of H_2O_2 to $HO^{\cdot}$ radicals, which react with hydroperoxo-Ti species to form superoxo-Ti and H_2O:

   $$H_2O_2 \rightarrow 2HO^{\cdot},$$

   $$\text{Ti–OOH} + HO^{\cdot} \rightarrow \text{Ti}(O_2^{-\cdot}) + H_2O.$$

   Formation of $HO^{\cdot}$ radicals by decomposition of H_2O_2 on contact with titanium silicates increases with temperature. At 77 K, this decomposition is less probable.
2. The second possibility is the dismutation of two superoxo ions to yield the peroxo species:

   $$O_2^{-\cdot} + O_2^{-\cdot} \rightarrow O_2^{2-} + O_2.$$

   Again, even if mobile superoxide ions were present in the sieve, they would not be able to diffuse at the low temperatures used for the EPR experiments (190–77 K).
3. The third possibility for the conversion of the superoxide to the peroxide is the homolytic opening of a cyclic peroxo species (more precisely $Ti^{4+}(O_2^{2-})$ to $Ti^{3+}(O_2^{-\cdot})$) as proposed by Notari [1]. Formation of Ti^{3+} species was indeed observed in the presence of a base, like NaOH (spectrum not shown), but in the neutral or acidic pH conditions, the Ti^{3+} species was not observed. Either their concentration, if formed, is very low or they are short-lived.

Table 3
Catalytic activity of titanosilicates in styrene epoxidation using aqueous H_2O_2 (HP) and urea–H_2O_2 adducts (UHP)[a]

Catalyst	Solvent	Oxidant	TOF (h^{-1})	Conversion (mol%)	Epoxide selectivty (mol%)	Ref.
TS-1	CH_3CN	HP	1.6	56.8	4.1	[30]
	$(CH_3)_2CO$	HP	2.1	76.8	6.2	
	CH_3OH	HP	2.5	88.8	0.6	
	CH_3CN	UHP	1.0	51	82	[19]
	$(CH_3)_2CO$	UHP	1.4	71	87	
	CH_3OH	UHP	1.1	54	72	
Ti-β	CH_3CN	UHP		51	60	This work
	$(CH_3)_2CO$	UHP	1.6	56	62	
	CH_3OH	UHP		60	51	
Amorphous Ti–SiO_2	$(CH_3)_2CO$	UHP	0.6	24	39	This work
TiMCM-41	$(CH_3)_2CO$	UHP	0.8	18	24	

[a] Reaction conditions: styrene/oxidant (mol/mol) = 4; styrene/solvent (wt/wt) = 1; reaction time, 12 h; catalyst wt, 20 wt% of the substrate; temperature, 313 K.

4. The concentration of the Ti($O_2^{-\cdot}$) species is solvent dependent. Thus solvent (or H_2O) may play the role of a redox partner.

The HO$^{\cdot}$ radicals, generated from the decomposition of H_2O_2, cause, perhaps, the hydroperoxo/peroxo to superoxo conversion. The superoxo species (the O–O stretching absorption near 1120–1150 cm^{-1}) could not be seen in the FT-IR spectrum [13] perhaps due to the dominant stretching and bending modes of water in the same region.

3.4. Styrene epoxidation and structure–activity relationships

Table 3 lists the catalytic activity data of different titanosilicates in styrene epoxidation. The reactions with urea–H_2O_2 as the oxidant yielded styrene epoxide (SO) more selectively (Table 3). On the contrary, with aqueous H_2O_2, phenylacetaldyhyde and benzaldehyde were produced as major products with smaller amounts of styrene epoxide. The conversion and SO selectivity (with urea–H_2O_2) varied in the order: TS-1 > Ti-β > amorphous Ti–SiO_2 > TiMCM-41. Over TS-1, the selectivity for SO in different solvents decreased in the following order: $(CH_3)_2CO$ > CH_3CN > CH_3OH. The epoxide selectivity was low with H_2O_2 due to the formation of isomerized and/or cleaved secondary products. The oxirane ring is prone to acid-catalyzed isomerization and hydrolysis in the presence of water (coming from aqueous H_2O_2). This problem is overcome when using urea–H_2O_2 (an anhydrous source of H_2O_2), which slowly releases the anhydrous H_2O_2 into solution.

Controlled EPR experiments on TS-1 + H_2O_2 + alkene (styrene or allyl alcohol) at 333 K revealed that the superoxo-titanium species are consumed during the reaction (Fig. 12). Species A was consumed faster than species B (Fig. 12, curves a–d). At the end of 25 min, only the B type species

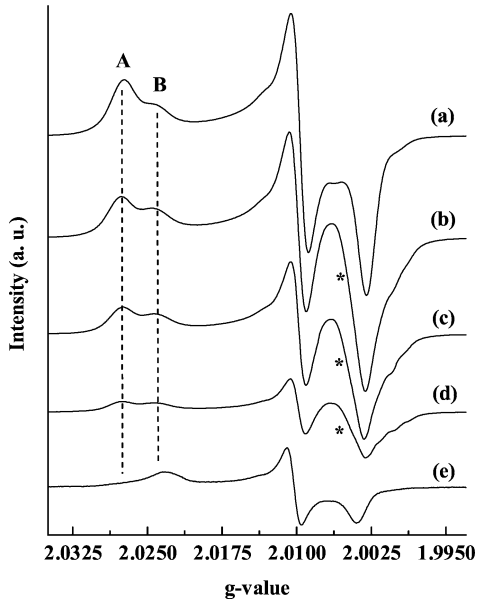

Fig. 12. Controlled EPR experiments on TS-1 + H_2O_2 + alkene at 333 K. Spectra were recorded at 90 K. TS-1 + H_2O_2 + styrene at (a) 0 min, (b) 5 min, (c) 10 min, (d) 20 min, (e) TS-1 + H_2O_2 + allyl alcohol (25 min). Asterisk represents signal due to a styrene-based radical formed during the reaction.

were observed with allyl alcohol (Fig. 12, curve e). With styrene as the substrate, organic radicals (represented by asterisks in Fig. 12) are formed during the reaction; their structure is not known at present. Such radicals were not observed in the reactions with allyl alcohol.

An attempt was made to correlate the relative EPR intensities of individual Ti($O_2^{-\cdot}$) species (A′, A, B, and C) in the various titanosilicates with their chemoselectivities in styrene oxidation. Fig. 13 presents the results. The relative concentration of A′ + A correlates with styrene oxide (SO) selectivity. Both the intensity of [A′ + A] signals and selectivity for SO were higher in TS-1 than in Ti-β (Fig. 13). The yield of nonselective products (phenyl acetaldehyde and benzaldehyde) correlates with the concentration of B + C. Similarly, the concentration of B + C is higher in CH_3OH solvent than in CH_3CN in parallel with the greater formation of nonselective products in the former than in the latter. Styrene epoxide concentration was *higher* when the total EPR signal intensity was *lower*. A comparison of our EPR data with the phenol hydroxylation activity data reported from our group earlier [31] indicates that the activity over titanosilicate catalysts increases directly with the total EPR signal intensity and more specifically with the total superoxo-titanium concentration. EPR-inactive hydroperoxo/peroxo-titanium species are, hence, probably responsible for epoxidation, while superoxo-titanium species are responsible for hydroxylation/oxidation reactions. Epoxidation reactions are more selective at lower temperatures. This greater selectivity for epoxidation at lower temperatures arises since, as noted from the variable temperature EPR studies, the hydroperoxo/peroxo-titanium species are more stable at

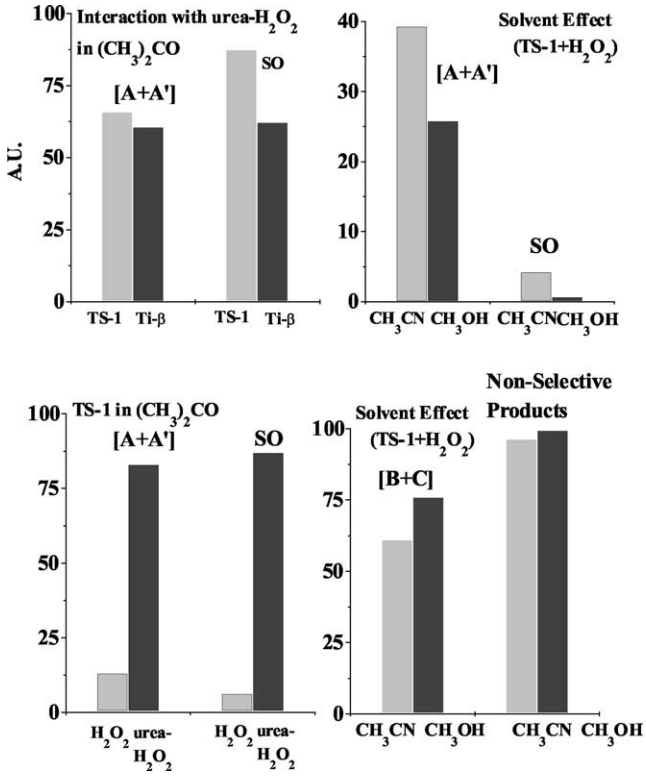

Fig. 13. Correlation between the intensity of $Ti(O_2^{-\bullet})$ ([A′ + A] and [B + C]) signals and selectivity of styrene oxide and nonselective products in styrene epoxidation reaction. The effects of titanosilicates, oxidants, and solvents on the correlation are depicted.

lower temperatures while the superoxo-titanium species are relatively more stable at higher temperatures. The EPR signal intensity in TiMCM-41 was lower when *tert*-butyl hydroperoxide in *n*-decane (rather than aqueous H_2O_2) was used as the oxidant, suggesting that a majority of oxo-titanium is in hydroperoxo/peroxo form in *n*-decane. A similar conclusion was also reached by Sankar et al. [9] but using the EXAFS/DFT techniques. The controlled EPR experiments reveal that the A-type species are consumed (EPR signal intensity decreased) during the reaction. Similar conclusions were drawn by Zhao et al. [17] in phenol hydroxylation where involvement of A-type superoxo in the reaction was claimed. The higher reactivity of A- compared to B-type species is, perhaps, due to its lability and easy conversion to hydroperoxo/superoxo species. The B-type species are in preponderance in TiMCM-41, amorphous Ti–SiO_2 and to some extent in Ti-β. The difference in the *type* of the preponderant oxo-titanium species present in the various titanosilicates, perhaps, explains the differences in their chemoselectivity (Table 3; catalytic selectivity varies in the order, TS-1 > Ti-β > amorphous Ti–SiO_2 > TiMCM-41).

4. Conclusions

The reactive oxygen intermediates generated in TS-1, Ti-β, amorphous Ti–SiO_2, and TiMCM-41, during interaction with aqueous H_2O_2 and urea–H_2O_2 adducts, were identified and quantified. The nature of the silicate structure, solvent, temperature, and oxidant influence the relative concentrations of these oxo-titanium species. The titanosilicates, in general, contain two types of oxo-titanium species A and B. The A-type species were generated from the tetrapodal $(SiO)_4Ti$ structures located in framework positions inside the pores of the catalyst, while the B-type species were from the tripodal $(SiO)_3Ti(OH)$ structures also located in the framework but most probably, at the external surface [8–10]. The former was predominant in TS-1 and Ti-β while the latter was predominant in amorphous Ti–SiO_2 and TiMCM-41, respectively. The A-type species exhibit greater selectivity for the epoxide (as compared to the B-type species) in styrene oxidation. The larger concentration of A-type species over TS-1, compared to Ti-β and TiMCM-41, may account for the greater chemoselectivity of the former in olefin epoxidations. Our EPR studies suggest the involvement of hydroperoxo-/peroxo-titanium in alkene epoxidations and superoxo-titanium in phenol hydroxylation/oxidation reactions. These structure–activity relations, in principle, can contribute to a better control of chemoselectivity in the titanosilicate system.

References

[1] B. Notari, Adv. Catal. 41 (1996) 253.
[2] B. Notari, Catal. Today 18 (1993) 163.
[3] G.N. Vayssilov, Catal. Rev.-Sci. Eng. 39 (1997) 209.
[4] A. Corma, Chem. Rev. 97 (1997) 2373.
[5] S. Pei, G.W. Zajac, J.A. Kaduk, J. Faber, B.I. Boyanov, D. Duck, D. Fazzini, T.I. Morrison, D.S. Yang, Catal. Lett. 21 (1993) 333.
[6] M.A. Camblor, A. Corma, J. Pérez-Pariente, J. Chem. Soc. Chem. Commun. (1993) 557.
[7] L. Marchese, T. Maschmeyer, E. Gianotti, S. Coluccia, J.M. Thomas, J. Phys. Chem. B 101 (1997) 8836.
[8] D. Gleeson, G. Sankar, C.R.A. Catlow, J.M. Thomas, G. Spanó, S. Bordiga, A. Zecchina, C. Lamberti, Phys. Chem. Chem. Phys. 2 (2000) 4812.
[9] G. Sankar, J.M. Thomas, C.R.A. Catlow, C.M. Barker, D. Gleeson, N. Kaltsoyannis, J. Phys. Chem. B 105 (2001) 9028.
[10] J.M. Thomas, G. Sankar, Acc. Chem. Res. 34 (2001) 571.
[11] F. Geobaldo, S. Bordiga, A. Zecchina, E. Giamello, G. Leofanti, G. Petrini, Catal. Lett. 16 (1992) 109.
[12] A. Zecchina, S. Bordiga, C. Lamberti, G. Ricchiardi, D. Scarano, G. Petrini, G. Leofanti, M. Mantegazza, Catal. Today 32 (1996) 97.
[13] G. Tozzola, M.A. Mantegazza, G. Ranghino, G. Petrini, S. Bordiga, G. Ricchiardi, C. Lamberti, R. Zulian, A. Zecchina, J. Catal. 179 (1998) 64.
[14] W. Lin, H. Frei, J. Am. Chem. Soc. 124 (2002) 9292.
[15] A. Tuel, J. Diab, P. Gelin, M. Dufaux, J.-F. Dutel, Y. Ben Taârit, J. Mol. Catal. 63 (1990) 95.
[16] A. Tuel, Y. Ben Taârit, Appl. Catal. A: Gen. 110 (1994) 137.
[17] Q. Zhao, X.-H. Bao, Y. Wang, L.-W. Lin, G. Li, X.-W. Guo, X.-S. Wang, J. Mol. Catal. A: Chem. 157 (2000) 265.
[18] K. Chaudhari, D. Srinivas, P. Ratnasamy, J. Catal. 203 (2001) 25.
[19] L. Bonoldi, C. Busetto, A. Congiu, G. Marra, G. Ranghino, M. Salvalaggio, G. Spanó, E. Giamello, Spectrochim. Acta 58A (2002) 1143.
[20] S.C. Laha, R. Kumar, J. Catal. 204 (2001) 64; J. Catal. 208 (2002) 339.
[21] R. Kumar, A. Bhaumik, R.K. Ahedi, S. Ganapathy, Nature 381 (1996) 298.

[22] R. Kumar, P. Mukherjee, R.K. Pandey, P. Rajmohanan, A. Bhaumik, Micropor. Mesopor. Mater. 22 (1998) 23.
[23] T. Blasco, M.A. Camblor, A. Corma, P. Esteve, J.M. Guil, A. Martínez, J.A. Perdigón-Melón, S. Valencia, J. Phys. Chem. B 102 (1998) 75.
[24] S.C. Laha, R. Kumar, Micropor. Mesopor. Mater. 53 (2002) 163.
[25] A. Keshavaraja, V. Ramaswamy, H.S. Soni, A.V. Ramaswamy, P. Ratnasamy, J. Catal. 157 (1995) 501.
[26] M. Anpo, M. Che, B. Fubini, E. Garrone, E. Giamello, M.C. Paganini, Top. Catal. 8 (1999) 189.
[27] M. Shiotani, G. Moro, J.H. Freed, J. Chem. Phys. 74 (1981) 2616.
[28] M. Che, A.J. Tench, Adv. Catal. 32 (1983) 1.
[29] H.C. Box, Electron Paramagnetic Resonance Spectroscopy, Academic Press, New York, 1997.
[30] A. Damin, G. Ricchiardi, S. Bordiga, F. Bonino, A. Zecchina, F. Ricci, G. Spanò, F. Villain, C. Lamberti, Stud. Surf. Sci. Catal. 135 (2001) 2394.
[31] S.B. Kumar, S.P. Mirajkar, G.C. Pais, P. Kumar, R. Kumar, J. Catal. 156 (1995) 163.